Molecular and Cellular Pathobiology

Cancer Research

EFA6B Antagonizes Breast Cancer

Joséphine Zangari[1], Mariagrazia Partisani[1], François Bertucci[2], Julie Milanini[1], Ghislain Bidaut[2], Carole Berruyer-Pouyet[2], Pascal Finetti[2], Elodie Long[3], Frédéric Brau[1], Olivier Cabaud[2], Bruno Chetaille[2], Daniel Birnbaum[2], Marc Lopez[2], Paul Hofman[3], Michel Franco[1], and Frédéric Luton[1]

Abstract

One of the earliest events in epithelial carcinogenesis is the dissolution of tight junctions and cell polarity signals that are essential for normal epithelial barrier function. Here, we report that EFA6B, a guanine nucleotide exchange factor for the Ras superfamily protein Arf6 that helps assemble and stabilize tight junction, is required to maintain apico-basal cell polarity and mesenchymal phenotypes in mammary epithelial cells. In organotypic three-dimensional cell cultures, endogenous levels of EFA6B were critical to determine epithelial–mesenchymal status. EFA6B downregulation correlated with a mesenchymal phenotype and ectopic expression of EFA6B hampered TGFβ-induced epithelial-to-mesenchymal transition (EMT). Transcriptomic and immunohistochemical analyses of human breast tumors revealed that the reduced expression of EFA6B was associated with loss of tight junction components and with increased signatures of EMT, cancer stemness, and poor prognosis. Accordingly, tumors with low levels of EFA6B were enriched in the aggressive triple-negative and claudin-low breast cancer subtypes. Our results identify EFA6B as a novel antagonist in breast cancer and they point to its regulatory and signaling pathways as rational therapeutic targets in aggressive forms of this disease. *Cancer Res; 74(19); 5493–506. ©2014 AACR.*

Introduction

Gene expression profiling has helped define five intrinsic tumor subtypes; essentially based on the expression of the two hormonal receptors, estrogen receptor (ER) and progesterone receptor (PR), and HER2. The triple-negative breast cancer (TNBC) subtype does not express any of these receptors, rendering it unsuitable for the hormonal and anti-HER2 treatments (1). TNBC is associated with low overall survival and high recurrence. Transcriptomic analyses have identified a new breast cancer subtype with poor prognosis named claudin-low (Cld-low), defined by the loss of expression of the proteins constitutive of the tight junction (2, 3). This subtype, which represents 12% of total breast cancer, is 75% TNBC, characterized by a core epithelial-to-mesenchymal transition (EMT) signature, and enriched in cancer stem cells (CSC), which are associated with relative resistance to conventional anticancer treatments.

We have reported that exchange factor for Arf6 (EFA6) contributes to the assembly and maintenance of the tight junction in the canine kidney cell line MDCK (4, 5). Four isoforms of EFA6 (A, B, C, and D) are encoded by separate genes (*PSD*, *PSD4*, *PSD2*, and *PSD3*, respectively). EFA6A, B, and D have ubiquitous expression while EFA6C is restricted to neuronal cells. We found that EFA6B levels increase at newly formed cell–cell contacts during epithelial polarity development to help promote tight junction assembly (4, 5). Once tight junctions are assembled, the levels of EFA6B decreases, yet at steady-state EFA6B still contributes to stabilize the tight junctions. Knockdown of EFA6B is sufficient to impair the assembly and stability of the tight junctions (5). Hence, the regulation of the levels of EFA6B proteins is key to tight junction homeostasis.

In this study, we have asked whether the EFA6B protein could act as an antagonist to malignant progression. To answer this question, we combined *in vivo* expression analyses in human breast tumor samples with *in vitro* approaches. On the basis of our results, we propose that EFA6B acts as an antagonist at the early stages of breast cancer development by hampering tight junction disassembly and loss of epithelial polarity.

Materials and Methods

Cells

MCF7, T47D, SKBR3, and MCF10A cells were obtained from the ATCC, authenticated by short-tandem repeat profiling by the vendor, and passaged for fewer than 6 months before experiments. Cells were grown in DMEM containing 10% FCS, except MCF10A cells grown in DMEM-F12, 5% horse serum,

[1]Institut de Pharmacologie Moléculaire et Cellulaire, Université de Nice Sophia-Antipolis CNRS UMR7275, Valbonne, France. [2]Centre de Recherche en Cancérologie de Marseille, INSERM UMR1068, Institut Paoli-Calmettes, CNRS UMR7258, Aix-Marseille Université, Marseille, France. [3]Laboratoire de Pathologie Clinique et Expérimentale et biobanque CHUN, Nice, France.

Note: Supplementary data for this article are available at Cancer Research Online (http://cancerres.aacrjournals.org/).

Corresponding Author: Frédéric Luton, Institut de Pharmacologie Moléculaire et Cellulaire, Université de Nice Sophia-Antipolis CNRS UMR7275, 660 route des Lucioles, 06560 Valbonne, France. Phone: 33-493957770; Fax: 33-493957708; E-mail: luton@ipmc.cnrs.fr

doi: 10.1158/0008-5472.CAN-14-0298

insulin, hydrocortisone, EGF, and cholera toxin (6). Transient transfection was performed by nucleofection (AMAXA) and stable transfection by lipofection using JETPEI (Polyplus Transfection). For stable expression of EFA6Bvsvg, cells were selected with Geneticin (Invitrogen) 2 days after transfection and low expressor clones were isolated. They all gave similar results in two-dimensional (2D) and three-dimensional (3D) culture assays. One clone was used in all the assays, and two other clones when randomly used in the different assays displayed similar results. When indicated, cells were grown on permeable filters (Costar) at 3×10^5 cells/12 mm filter. For 3D-cell culture, 2×10^3 cells were mixed with 25 μL of Matrigel (BD Biosciences) deposited as a drop on a 12-mm glass coverslip. MDCK-EFA6Bvsvg cells were described elsewhere (5). Before TGFβ treatment, the cells were serum-starved overnight and 10 μg/mL TGFβ (Sigma-Aldrich) was added for the indicated period of times.

DNA, siRNAs, and shRNAs

pEGFP-Arf6T27N and pcDNA3-EFA6Bvsvg were described elsewhere (7, 8). EFA6B was cloned into pEGFPC3 by PCR. The silencing mutations to generate a construct insensitive to the siRNAs were introduced using the QuickChange Mutagenesis Kit (Agilent Technologies). Extinction of EFA6B expression was obtained in MCF7 cells using a pool of four siRNA or in MCF10A, T47D, and SKNBR3 cells using a pool of three human EFA6B-specific shRNA cloned into the lentiviral vector pLB, independently expressing GFP (Addgene; #11619). Sequences of all the primers, siRNAs, and shRNAs are described in Supplementary Methods. The pWZL-Blast-mouse-E-cadherin lentiviral vector was obtained from Addgene (#18804; ref. 9).

Antibodies

Rabbit polyclonal sera specific for ZO-1, claudin-1, occludin (Invitrogen), EFA6B (Sigma-Aldrich), Smad2, and phospho-Smad2 (Ser465/467; Cell Signaling Technology), mouse monoclonals specific for E-cadherin, β-catenin, GM130 (BD Biosciences), RhoA (Santa Cruz Biotechnology), actin, and vsvg tag (Sigma-Aldrich), rabbit monoclonal specific for phospho-Ezrin/Radixin/Moesin (Cell Signaling Technology) were used. The mouse monoclonal anti-Arf6 was described elsewhere (10).

Transepithelial electrical resistance

The transepithelial electrical resistance (TER) was measured with an EVOM (WPI) using triplicates or quadruplicates for each measurement as previously described (11).

Immunofluorescence

Cells were fixed in paraformaldehyde, the samples processed as previously described (4) and imaged on a confocal microscope (Leica TCS-SP5). Tight junction length and fluorescence intensity quantifications were performed on the basis of the occludin fluorescence staining using a home-made ImageJ program described in details in Supplementary Methods (12).

Immunoblot

Cells were solubilized in SDS lysis buffer and the lysates were prepared for immunoblot as previously described (5). The proteins were revealed by chemiluminescence (Amersham) and the membranes were analyzed with the luminescent analyzer LAS-3000 (Fujifilm).

EFA6B/*PSD4* mRNA expression analysis in breast cancer samples

To determine *EFA6B*/*PSD4* mRNA expression in breast cancer samples and search for correlations with histoclinical and molecular features, we analyzed DNA microarray–based transcriptomic data. Expression in mammary cell lines was analyzed in our database of 43 cell lines profiled using our Affymetrix platform (U133 Plus 2.0; ref. 13). Expression in clinical tissue samples was analyzed in our series of 352 patients with invasive adenocarcinoma and four pools of normal breast tissue samples (11 healthy women), and in 32 public datasets collected from the National Center for Biotechnology Information/Genbank Gene Expression Omnibus (GEO) database, the European Bioinformatics Institute ArrayExpress database, or at the authors' websites (Supplementary Table S1). This resulted in a total of 5,252 nonredundant primary invasive breast cancers with both *EFA6B*/*PSD4* mRNA expression and histoclinical data available for analysis. For the Agilent-based datasets, we applied quantile normalization to available processed data. Regarding the Affymetrix-based datasets, we used robust multichip average (RMA) with the nonparametric quantile algorithm as normalization parameter. Comparison of mean *EFA6B*/*PSD4* mRNA expression level according to classical histoclinical factors was done using Student *t* test. To compare the distribution according to categorical variables, we used the Fisher exact test. All statistical tests were two-sided at the 5% level of significance. Statistical analysis was done using the survival package (version 2.30) in the R software. We followed the reporting REcommendations for tumor MARKer prognostic studies (REMARK criteria). A fully detailed description of the methods and statistical procedures is provided in Supplementary Methods.

Immunohistochemical expression of EFA6B and claudin-3 in breast cancer samples

A total of 412 human primary invasive breast adenocarcinoma were analyzed by immunohistochemistry (IHC) using tissue microarray (TMA). Using a TMA instrument (Beecher Instruments), three representative areas of each tumor were punched from the archival paraffin-embedded formalin-fixed tissue blocks. IHC was performed on serial 4-μm deparaffinized TMA sections using an automated single-staining procedure. The extent of EFA6B and claudin-3 immunostaining signals was expressed semi-quantitatively as the sum of scores representing the proportion and staining intensity of negative and positive tumor cells. The score of the immunoreactivity for the two proteins was tested for correlation with traditional clinicopathologic parameters by using the χ^2 test for categorical variables, and the Mann–Whitney *U* test for continuous variables. The coefficient of correlation (ρ) between variables was calculated using the Spearman rank test. Association between protein levels and survival was calculated using the Kaplan–Meier method and curves were compared with the log-rank test. The collection of breast cancer samples, detailed

methods, and statistical procedures are described in Supplementary Methods.

Results

Exogenous expression of EFA6B in MCF7 cells restores a normal polarized epithelial monolayer with functional tight junction

To address the role of EFA6B on breast cancer development, we first asked whether the exogenous expression of EFA6B would enable tumoral mammary cells to assemble a functional tight junction. We chose to study the MCF7 cells because it is the only human mammary tumoral cell line known to assemble, although very partially, a tight junction. Owing to their weakly tumoral phenotype, they adopt an incomplete polarized morphology when grown on filters and an unpolarized compact cell cluster organization under 3D-culture conditions (14, 15). After stable transfection of EFA6Bvsvg, we selected subclones with no more than five times the level of the endogenous protein (Fig. 1B). At this level of expression, EFA6Bvsvg remained localized at the apical pole of the cells consistent with our previous observations for the endogenous protein in MDCK cells (Fig. 1A; ref. 4). When grown to confluence on filters, about 10% of MCF7 cells organized in small patches of 5 to 10 cells that assembled a tight junction. In contrast, MCF7 cells expressing EFA6Bvsvg (MCF7-EFA6Bvsvg) demonstrated consistent assembly of a continuous tight junction throughout the entire monolayer. The adherens junctions correctly assembled and were not affected by EFA6Bvsvg expression (Fig. 1A and Supplementary Fig. S1A and S1B). The expression of EFA6Bvsvg did not alter the levels of expression of the components of the tight junction, nor those of the adherens junction, nor the substrate of EFA6B, Arf6 (Fig. 1B). An automated quantification based on occludin staining showed that tight junction size and mean intensity increased at least three and four times, respectively (Fig. 1C). The assembled tight junctions were functional as MCF7-EFA6Bvsvg gained TER faster than control cells with a 3.2-fold increase at day 3 (Fig. 1D). More strikingly, the MCF7-EFA6Bvsvg cells adopted characteristics of a well-differentiated apico-basal epithelial morphology: (i) regular cuboidal cells organized as a monolayer, (ii) apical punctate actin staining typical of the microvilli of polarized cells, (iii) nuclei regularly aligned basally, (iv) adherens junction proteins restricted to the lateral cell–cell contacts, (v) apical tight junction proteins (Fig. 1A and Supplementary Fig. S1A and S1B). In contrast, MCF7 cells displayed a heterogeneous and rather round morphology, tended to form multilayers, displayed a continuous plasma membrane staining of the adherens junctions all around the cell, and formed little tight junctions and no microvilli (Fig. 1A and Supplementary Fig. S1A and S1B). Thus, expression of EFA6Bvsvg is sufficient to elicit an epithelial transition of the MCF7 cells from their intermediate epithelio-mesenchymal phenotype.

Exogenous expression of EFA6B in MCF7 cells induces a phenotypic reversion in 3D culture

Although 2D culture on porous filters is best suited to analyze the formation and barrier function of the tight junction, 3D-organotypic cell culture where cells organize as acini is more appropriate to assess the luminogenic and polarizing capacities of epithelial cells. As previously described, in 3D culture, MCF7 cells formed aggregates with no radial symmetry and random nuclei distribution; a phenotype named "mass" representative of rather weakly tumoral mammary cell lines (14, 15). The F-actin staining was stronger in peripheral membrane protrusions (Fig. 1E), and the rare lumens were virtually always between just two cells. In contrast, EFA6Bvsvg expression stimulated lumen formation and MCF7-EFA6Bvsvg cells organized as nearly normal mammary acini-like structures (Fig. 1E and Supplementary Fig. S1C and S1D) comparable with those obtained with the normal mammary epithelial MCF10A cells (data not shown; refs. 14, 15). The quantification of the number of aggregates containing at least one lumen showed a 3-fold increase in MCF7 cells when expressing EFA6Bvsvg; few lumens were formed just in between two cells (Fig. 1F). Most lumens were connected to multiple cells to form either one central lumen (9.4%), or two large lumens (62.5%) and sometimes three or more lumens (28.1%). Regardless of the number of lumens, within the cysts each individual cell was connected to a lumen and perfectly polarized. Their apical surface facing the lumen displayed a strong actin staining colabeled for the apical phosphorylated proteins of the ERM family (Fig. 1E and Supplementary Fig. S1C and S1D). The adherens junction proteins were restricted to the lateral surface and the tight junction markers confined to the apex of the lateral membrane delineating the apical domain (Fig. 1E and Supplementary Fig. S1C and S1D). Finally, the Golgi apparatus was positioned above the nucleus, consistent with the correct orientation of the apico-basal axis (Supplementary Fig. S1D). Thus, EFA6Bvsvg expression is not only capable of facilitating the assembly of the tight junction, it also promotes the reversion to an epithelial phenotype, resulting in cells organizing collectively into normal mammary acini-like structures. This property was totally blocked upon coexpression of the dominant-negative Arf6T27N-GFP (Fig. 1G), indicating that EFA6B effects are dependent on Arf6 activation.

EFA6B contributes to the formation and fusion of VACs to generate lumens in polarized MCF7 acini

Although, MCF7 cells do not form acinis, they do form aggregates, indicating that the limiting step to make normal acinis is likely the ability to form lumens. Thus, we investigated how MCF7-EFABvsvg cell formed their lumens. When grown on coverslips and stained for F-actin, we observed that a higher proportion of cells overexpressing EFA6Bvsvg contained large intracellular vacuoles reminiscent of the vacuolar apical compartments (VAC) as well as small lumens formed in between two and four cells. Several VACs could be observed in certain cells, and VACs were already visible at the two-cell stage (Fig. 2A). VACs share characteristics with the apical plasma membrane displaying microvilli and containing apically, but not basolaterally, targeted proteins. VACs are proposed to fuse to cell–cell contacts to form the apical membrane (16–18). Quantification of cell aggregates grown in 3D culture showed that MCF7-EFA6Bvsvg contained three times more VACs and five times more lumens than control MCF7 cells (Fig. 2F). The lumens formed in MCF7-EFA6Bvsvg cells displayed the typical

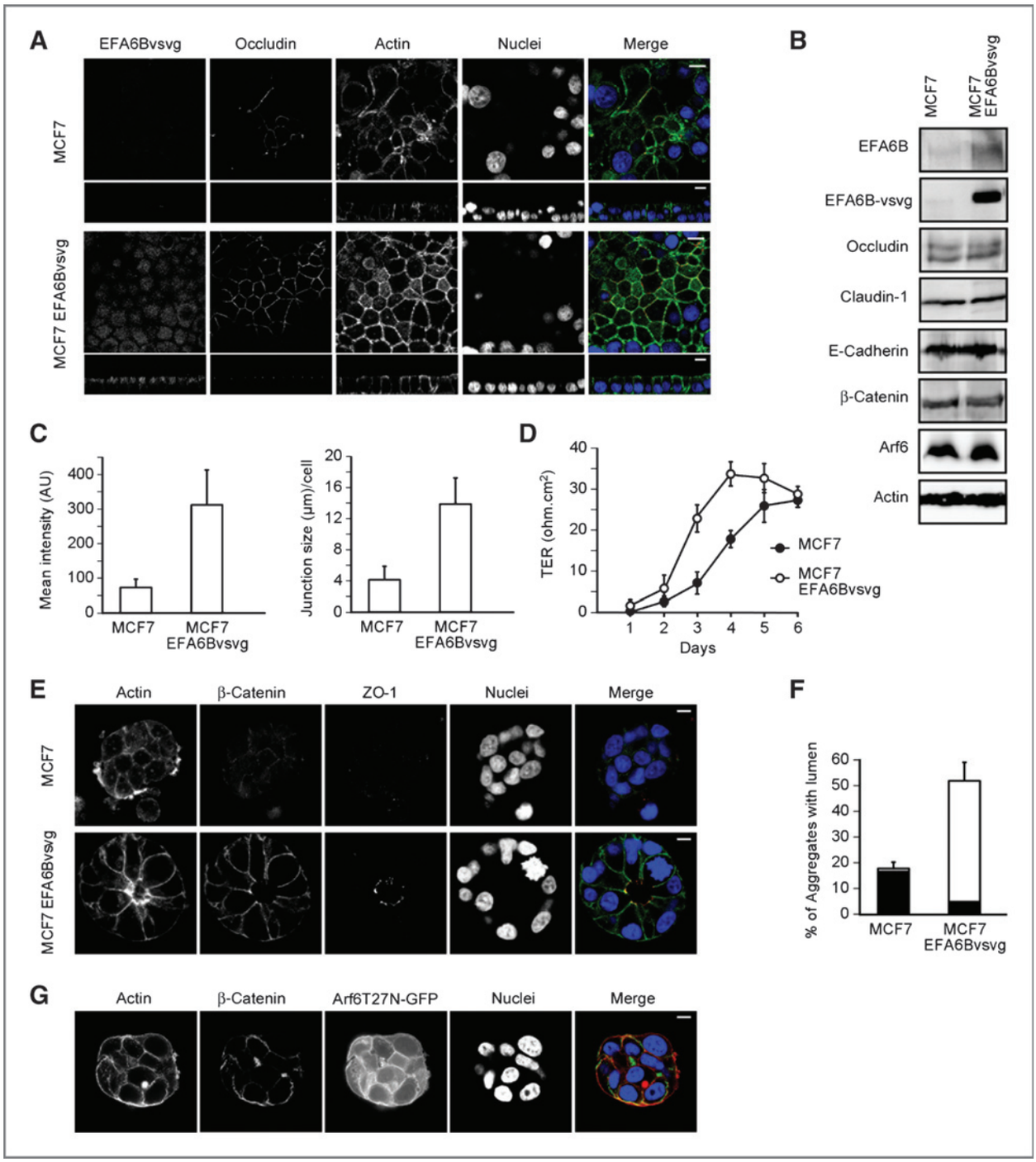

Figure 1. Expression of EFA6Bvsvg restores normal apico-basal polarity in MCF7 cells. A, cells grown on filters for 5 days were processed for immunofluorescence analysis and labeled for the indicated markers. Individual images of horizontal sections at the level of the cell junctions and vertical sections are shown. The merged images combine staining for occludin, actin, and nuclei. B, immunoblot analysis of the indicated proteins in cells grown on filters for 5 days. C, quantification of the mean intensity and size of the tight junction stained for occludin. $n = 5$, average ±SD, Student t test P values for mean intensity and junction size were <0.005. D, TER measurement. $n = 4$, average ±SD, Student t test P values at days 3 and 4 were <0.005. E, cells grown in Matrigel for 7 days were processed for immunofluorescence analysis and labeled for the indicated markers. Individual images across cell aggregates are shown individually and as colored merged images that combine staining for β-catenin, ZO-1, and nuclei. F, quantification of the number of acini containing at least one lumen at day 7 of growth in Matrigel. The inner black boxes indicate the proportion of lumen in between just two cells. $n = 6$, average ±SD, Student t test, $P < 0.001$. G, MCF7EFA6Bvsvg cells transfected for the expression of Arf6T27N-GFP were grown in Matrigel for 7 days, processed for immunofluorescence analysis, and labeled for the indicated markers. Individual images across the aggregates are shown individually and as a colored merged image that combines staining for actin, β-catenin, and nuclei. Scale bar, 10 μm.

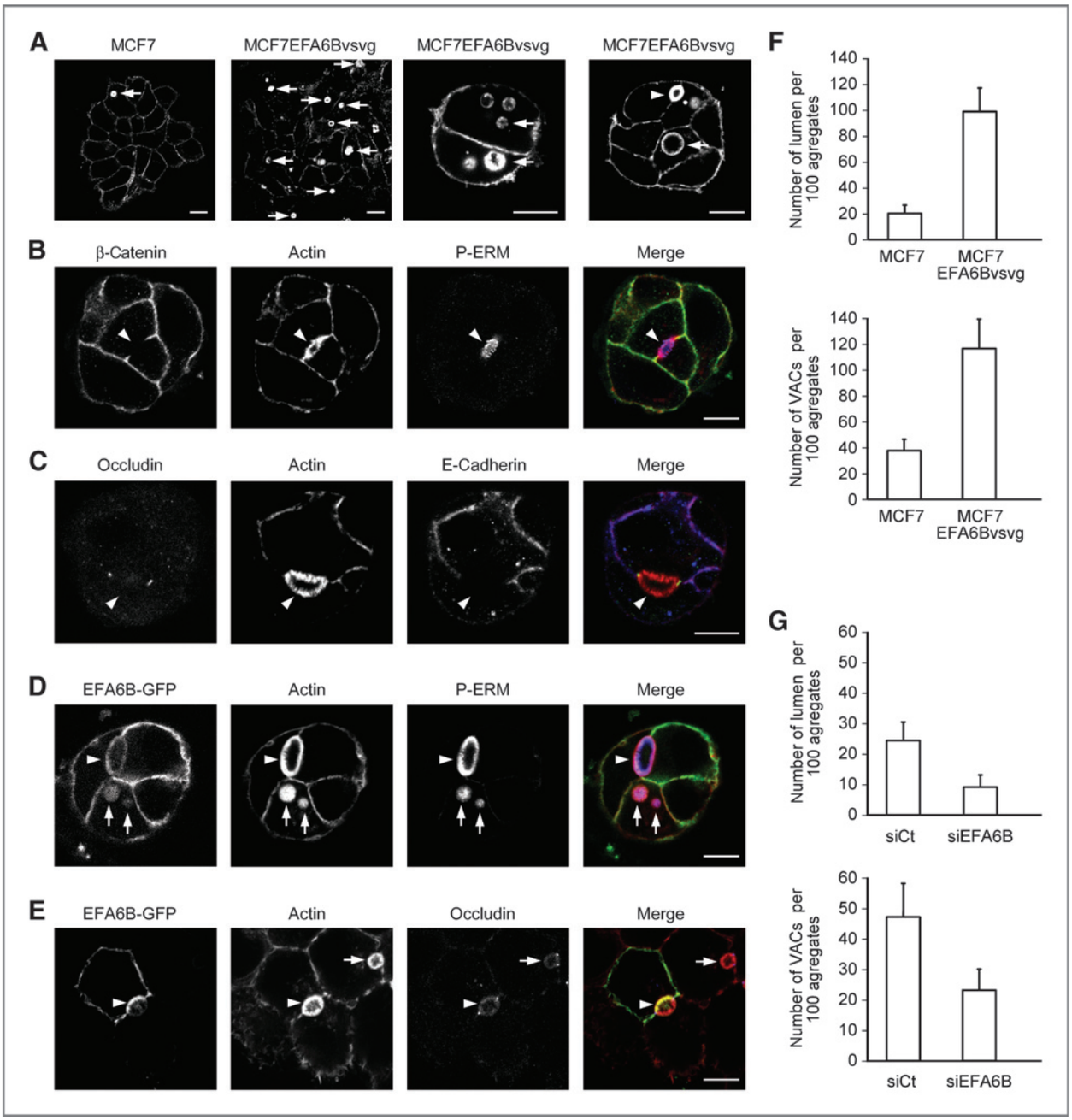

Figure 2. EFA6B promotes lumen formation in MCF7 polarized acini. A, MCF7 and MCF7EFA6Bvsvg cells were grown on coverslips and stained for F-actin. MCF7EFA6Bvsvg (B and C) and MCF7EFA6B-GFP (D) cells grown in Matrigel for 5 days were processed for immunofluorescence analysis and labeled for the indicated markers. E, MCF7 and MCF7EFA6B-GFP cells were mixed and grown in Matrigel for 3 days, processed for immunofluorescence analysis, and labeled for the indicated markers. B–E, individual images across cell aggregates are shown individually and as colored merged images. Arrows point to VACs and arrowheads to lumens. Scale bar, 10 μm. F, quantification of the number of lumens and VACs at day 5 of growth in Matrigel. $n = 4$, average ±SD, Student t test P values for lumens and VACs were <0.001. G, quantification of the number of lumens and intracellular VACs in MCF7 cells transfected with control (siCt) or EFA6B-specific siRNA at day 5 of growth in Matrigel. $n = 4$, average ±SD, Student t test P values for lumens and VACs were <0.005.

characteristics of an apical plasma membrane with actin-rich microvilli, selective staining for apical markers such as the P-ERM proteins (Fig. 2B), absence of the basolateral proteins β-catenin and E-cadherin (Fig. 2B and C), and surrounded by a tight junction ring (Fig. 2C). To assess EFA6B localization during luminogenesis, we generated a stable MCF7 cell line expressing EFA6BGFP. Interestingly, at early stages, EFA6BGFP was found at the cell surface, then on the VACs and at the apical plasma membrane (Fig. 2D). To confirm that the lumens were formed by fusion of the VACs with the plasma

membrane, we mixed MCF7-EFA6BGFP and MCF7 control cells. We observed that whole lumens stained for F-actin and P-ERM were made of one half labeled with EFA6BGFP and the other half unlabeled. Thus, upon fusion, the VACs provide one half of the lumen, the other half being formed on the other side by the facing cell (Fig. 2E). In addition, upon fusion of the VACs, the new lumens were rapidly limited to the cell–cell contact by a ring of tight junction (Fig. 2E).

Wild-type MCF7 cells form typical VACs and small lumens albeit essentially seen in between two cells (Fig. 1F and Supplementary Fig. S1E). We asked whether the endogenous EFA6B was also necessary to generate these VACs and small lumens. We used a pool of four siRNAs that specifically downregulated EFA6B but not the other EFA6 isoforms expressed in MCF7 cells, EFA6A and EFA6D (Supplementary Fig. S2A and S2B). We observed that siRNA knockdown of EFA6B led to half fewer VACs and three times less lumens (Fig. 2G).

Collectively, our results showed that EF6AB is involved in the formation and fusion of the VACs to form lumens within MCF7 cell aggregates, providing a mechanistic explanation as to how EFA6B contributes to the epithelial phenotypic reversion of MCF7 cells in 3D culture.

EFA6B repression in MCF7 cells abrogates the assembly of tight junctions and leads to highly unorganized aggregates

Next, we analyzed the effects of EFA6B downregulation by siRNA. When grown on filters, EFA6B-depleted cells displayed a less organized phenotype with a higher propensity to form multilayers. No tight junction formation was observed, although the adherens junction was unaffected as well as the total amount of tight junction proteins (Fig. 3A–C), indicating that EFA6B is regulating the tight junction assembly *per se* as previously observed in MDCK cells (4, 5). When grown in Matrigel, the aggregates became much less compact and appeared multilobular reminiscent of the "grape-like" morphotype typically found in advanced tumoral cell lines (14, 15). In these unorganized aggregates, adherens junction staining was still visible while the tight junction and the apical membrane domain were absent (Fig. 3D). The proportion of grape-like aggregates was reduced upon EFA6Bvsvg expression and increased in EFA6B knockdown cells. As a consequence, the percentage of aggregates with lumen(s) was proportionally reduced in EFA6B knockdown cells (Fig. 3E and F). The specificity of EFA6B knockdown was verified by a rescue experiment in which the effects of the depletion of the endogenous EFA6B protein by siRNA were reverted by the coexpression of a siRNA-insensitive EFA6B construct (Supplementary Fig. S2C and S2D). In conclusion, while overexpression of EFA6B supports the epithelial phenotype, downregulation of endogenous EFA6B promotes the mesenchymal phenotype.

EFA6B repression disturbs the epithelial phenotype of MCF10A, T47D, and SKBR3/E-cadherin cells

We then assessed the effects of EFA6B depletion on the collective organization of other human mammary cell lines grown in Matrigel. Normal mammary epithelial cells, MCF10A, were analyzed at early-stage aggregate formation and after luminogenesis. At early stages, wild-type and pLB-transduced cells formed round structures composed of rather cuboidal cells organized as a regular peripheral layer surrounding the inner cells of the aggregates. In contrast, EFA6B knocked down cells formed irregularly shaped structures of the "mass" type made of round and heterogeneous cells, similar to MCF7 aggregates (Fig. 4A–C). At later stages, EFA6B depletion did not prevent the cells from eventually forming a single central lumen, most likely because MCF10A cells do not form their lumen by exocytosis of VACs, but by cavitation, a process dependent on apoptosis (19), which we found not to be affected by EFA6B levels of expression (data not shown). Next, we studied the T47D cell line that is similar to MCF7 (ER/PR$^+$, HER2-low) with an intermediate epithelial–mesenchymal phenotype although they do not assemble any tight junction. As previously reported (14, 15), T47D wild-type as well as pLB-transduced cells adopted the "mass" phenotype. Similarly to MCF7, upon depletion of EFA6B, T47D cells no longer formed round and compact aggregates but rather unorganized loose structures (Fig. 4D–F). Subsequently, we studied the more tumoral cell line SKBR3 (ER/PR$^-$, HER2-high) that does not express E-cadherin and organizes as archetypical grape-like structure (14, 15). However, upon exogenous expression of E-cadherin, SKBR3 cells were shown to organize in the "mass" phenotype (Fig. 4G–I; ref. 20). Although knockdown of EFA6B in SKBR3 cells did not affect their grape-like phenotype (data not shown), EFA6B knocked down in SKBR3/E-cadherin cells reverted the "mass" phenotype back to a grape-like phenotype. This result supports our previous observations that EFA6B acts downstream of E-cadherin to regulate the tight junction assembly and epithelial cell polarization (4, 5). Altogether, our results demonstrate that EFA6B expression is required for the proper collective organization of mammary epithelial cells.

Exogenous expression of EFA6Bvsvg abrogates the TGFβ-induced EMT

We showed that increasing EFA6Bvsvg expression supports the epithelial phenotype, whereas reciprocally repression of EFA6B promotes the mesenchymal phenotype, suggesting that EFA6B might regulate the EMT. TGFβ is a major inducer of EMT during mammary gland morphogenesis and breast cancer progression (21–23). TGFβ induces early on the disassembly of the tight junction to which the TGFβ receptor (TGFβR) is physically associated through the polarity protein Par6 and occludin (24–27). When MCF7 cells were exposed to TGFβ, they downregulated the expression of E-cadherin and occludin, without affecting the endogenous EFA6B (Fig. 5A and B). This was accompanied by a major change in cell morphology with the apparition of stress fibers and an elongated cell shape (Fig. 5C). In contrast, MCF7-EFA6Bvsvg cells did not respond to TGFβ treatment (Fig. 5A and C). The expression of EFA6Bvsvg did not alter the levels of expression of TGFβR, thus the inhibitory effect of EFA6Bvsvg was not due to a decrease in the expression of TGFβR (data not shown). The inhibitory effect of EFA6B was totally blocked upon coexpression of the dominant-negative Arf6T27N-GFP (Fig. 5D). Note that in those cells, as in MCF7 cells expressing Arf6T27N-GFP (data not shown), stress fibers were no longer observed even upon TGFβ

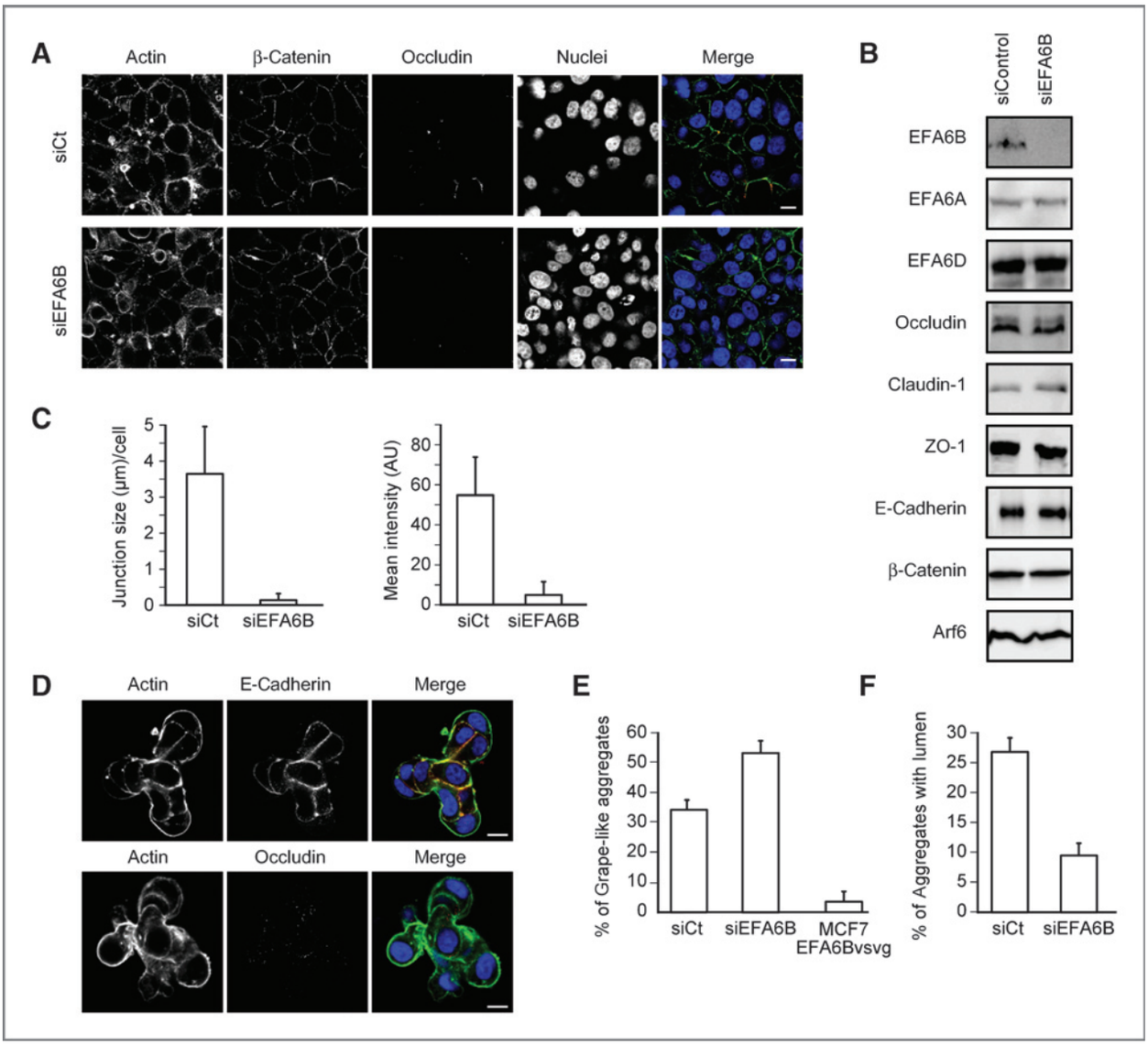

Figure 3. EFA6B repression in MCF7 cells abrogates the assembly of tight junction and leads to unorganized aggregates. A, the indicated cells were grown on filters for 5 days, processed for immunofluorescence analysis, and labeled for the indicated markers. Individual images of horizontal sections at the level of the cell junctions are shown individually and as colored merged images that combine staining for β-catenin, occluding, and the nuclei. B, immunoblot analysis of the indicated proteins in cells grown on filters for 5 days. C, quantification of the mean intensity and size of the tight junction stained for occludin in cells grown on filters for 5 days. $n = 3$, average ±SD, Student t test P values for mean intensity and junction size were <0.001. D, MCF7 cells transfected with EFA6B-specific siRNA were grown in Matrigel for 5 days, processed for immunofluorescence analysis, and labeled for the indicated markers. Individual images across cell aggregates are shown individually and as colored merged images. E, quantification of grape-like aggregates in the indicated cells. $n = 3$, average ±SD, Student t test P values for siEFA6B and MCF7EFA6Bvsvg cells to the siRNA control cells were <0.001 and 0.0005, respectively. F, quantification of the number of aggregates with lumens at day 6 of growth in Matrigel in the indicated cells. $n = 3$, average ±SD; Student t test, $P < 0.001$. Scale bar, 10 μm.

treatment. Nevertheless, the change in morphology and drop of E-cadherin expression were clearly apparent, indicating that Arf6 activation is required to hamper the TGFβ-induced EMT. To assess whether this inhibitory effect was cell-specific, we analyzed the non-mammary epithelial MDCK cell line. Like in MCF7 cells, in MDCK cells overexpressing EFA6Bvsvg the morphologic changes and the decrease in the levels of E-cadherin and occludin in response to TGFβ were totally blocked (Supplementary Fig. S4).

Induction of EMT by TGFβ is believed to take place through the activation of the canonical SMAD pathway that transduces gene expression program, and noncanonical pathways responsible for the rapid morphologic changes including the Par6, PI3K, and ERK pathways (23, 28). We observed a steady increase in Smad2 phosphorylation in both MCF7 and MCF7-EFA6Bvsvg cells, indicating that EFA6Bvsvg did not affect the SMAD pathway (Fig. 5E). TGFβ induces the disassembly of the tight junction by downregulating the levels of RhoA through Par6 and

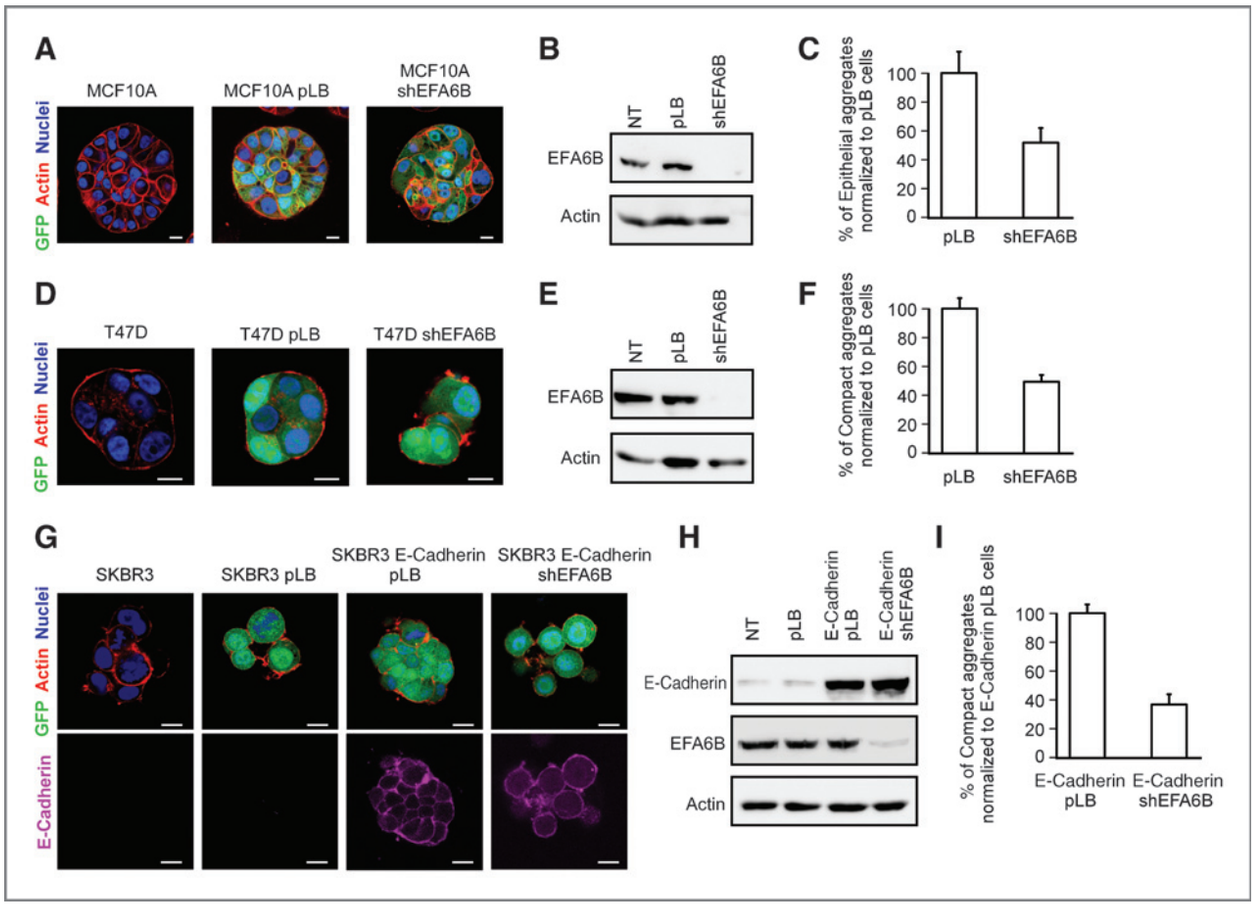

Figure 4. EFA6B repression disturbs the epithelial phenotype of MCF10A, T47D, and SKBR3/E-cadherin cells. EFA6B repression was achieved by lentiviral transduction of a pool of three EFA6B-specific shRNA. The empty vector was used as a control. Cell transduction was monitored by GFP expression. A, D, and G, the indicated cells grown in Matrigel for 5 to 7 days were processed for immunofluorescence analysis. Individual images across cell aggregates are shown as colored merged images of the indicated markers. For SKBR3 cells, an image of the exogenously expressed E-cadherin is shown separately. Scale bar, 10 μm. B, E, and H, immunoblot analysis of EFA6B knockdown in the indicated cell lines. C, F, and I, quantification of the epithelial morphology of the aggregates formed by the indicated cell lines. At least 100 aggregates of each cell line were classified according to their phenotype either resembling the pLB or shEFA6B phenotype shown on the images. For comparison purpose, the data were normalized to each cell line transduced with the lentiviral pLB empty vector. Average ± SD, Student *t* test *P* values in C ($n = 3$), F ($n = 4$), and I ($n = 4$) were <0.01, <0.005, and <0.005, respectively.

the ubiquitin-ligase Smurf1 (26). Similarly to previous reports (29, 30), we found a transient but reproducible decrease in the levels of RhoA after 30-minute exposure to TGFβ, which was comparable in both cell lines, indicating that EFA6Bvsvg did not act through RhoA downregulation (Fig. 5E). MCF7 cells carry an activating mutation of the *PIK3CA*, leading to a constitutive phosphorylation of its downstream effector Akt (31, 32). This constitutive phosphorylation was unaffected by EFA6Bvsvg expression and we could not detect further phosphorylation upon TGFβ treatment in either cell lines. Similarly, ERK1/2 phosphorylation was not increased by TGFβ in MCF7 and MCF7EFA7Bvsvg cell lines (data not shown). Collectively, our data indicate that EFA6Bvsvg inhibits the TGFβ-induced EMT through a yet unidentified mechanism.

EFA6B/*PSD4* mRNA expression in breast cancer

The fact that EFA6B regulates the tight junction assembly, apico-basal polarity, and inhibits the TGFβ-induced EMT led us to determine whether EFA6B might act as an antagonist to mammary tumoral progression *in vivo*. A recent transcriptomic analysis revealed the existence of a new subtype of breast cancer called Cld-low characterized by the loss of expression of the tight junction components (2). Thus, we postulated that loss of EFA6B expression could contribute to the downregulation of the tight junction during tumoral progression. Analysis of *EFA6B* mutations and copy number alterations from the cBioPortal website (33) showed a very low alteration rate (0.2%) in breast cancer (Supplementary Fig. S5). Then, we analyzed the mRNA expression level of *EFA6B*/*PSD4* in our collection of 43 human mammary cell lines previously profiled using DNA microarrays and of which 14 are characterized as Cld-low. *EFA6B*/*PSD4* expression was lower in Cld-low cell lines than in non–Cld-low cell lines ($P < 0.001$, Student *t* test; Fig. 6A). Subsequently, we measured the expression levels of *EFA6B*/*PSD4* in our large dataset of 5,252 invasive breast carcinomas (Supplementary Table S1). From this cohort, a

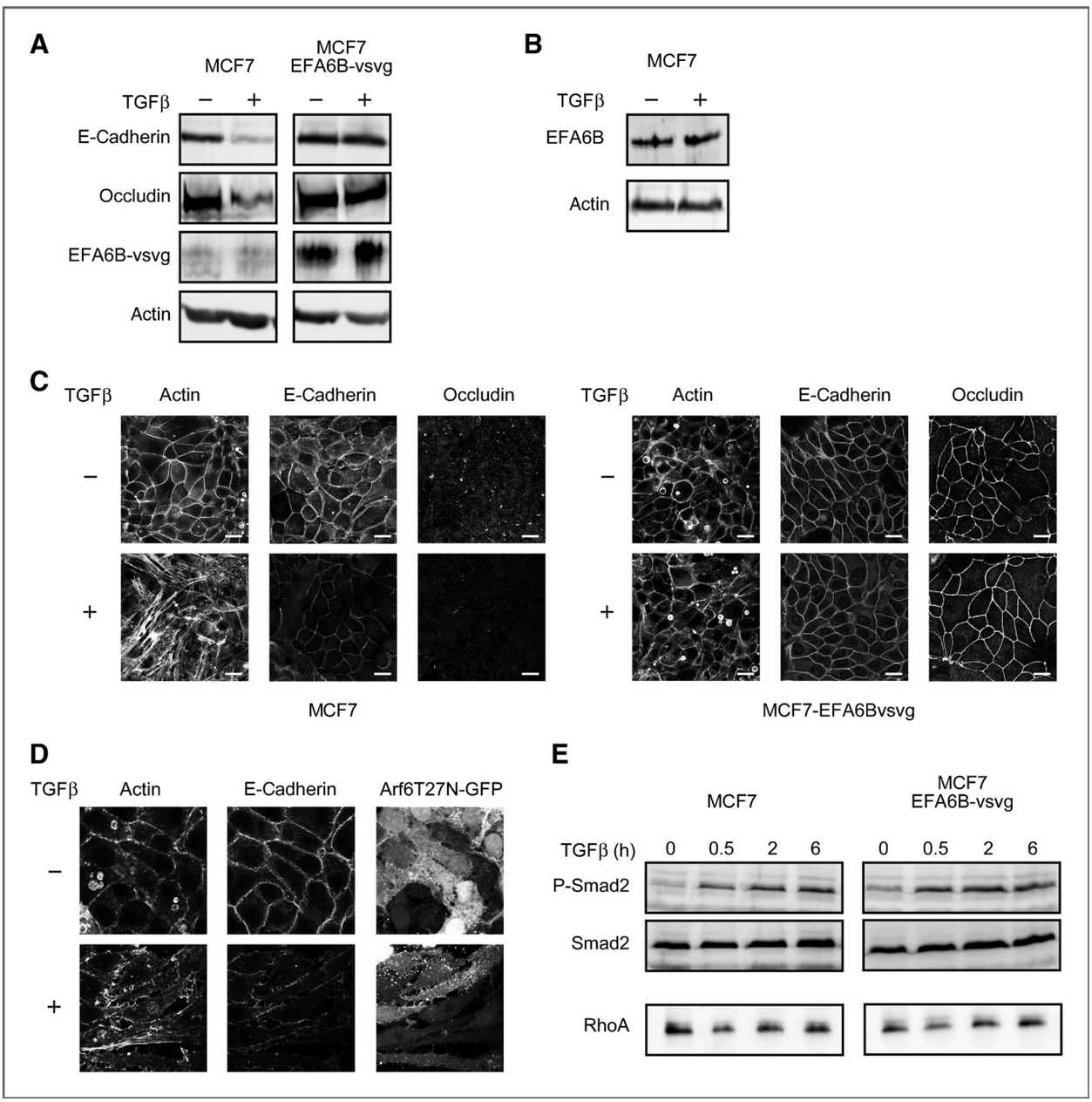

Figure 5. Expression of EFA6Bvsvg in MCF7 cells abrogates the TGFβ-induced EMT. Cells exposed or not to 10 μg/mL of TGFβ for 3 days were analyzed for the expression of the indicated proteins by immunoblot (A and B) or processed for immunofluorescence and stained for the indicated markers (C). Individual images of horizontal sections at the level of the cell junctions are shown. D, immunoblot analysis of the indicated proteins in cells exposed to TGFβ (10 μg/mL). E, the MCF7-EFA6Bvsvg cell line was transiently transfected with a vector encoding Arf6T27N-GFP and studied for its response to TGFβ. Scale bar, 10 μm.

total of 500 tumors showed a 2-fold or greater upregulation and 281 showed a 2-fold or greater downregulation of *EFA6B*/*PSD4*, using normal breast tissue as the standard. Correlation analysis between *EFA6B*/*PSD4* expression and histoclinical features of tumors (Table 1) showed that *EFA6B*/*PSD4* downregulation was associated (Fisher exact test) with higher grade ($P < 0.001$), higher frequency of ER^- status ($P < 0.001$), PR^- status ($P < 0.001$), triple-negative status ($P < 0.001$), and more frequently basal ($P < 0.001$) and Cld-low subtypes ($P < 0.001$). Correlation also existed with disease-free survival (DFS) within the 2,930 non–stage IV patients with follow-up available. A total of 1,056 patients experienced a disease event, and 1,874 remained disease-free after a median follow-up of 82 months. The 5-year metastasis-free survival (MFS) was 67% [95% confidence interval (CI), 65%–69%] for the whole population, and 54%, 67%, and 76% in cases of downregulation, no deregulation, and upregulation, respectively (Fig. 6B). Importantly, for all of the histoclinical correlations described above, a continuum

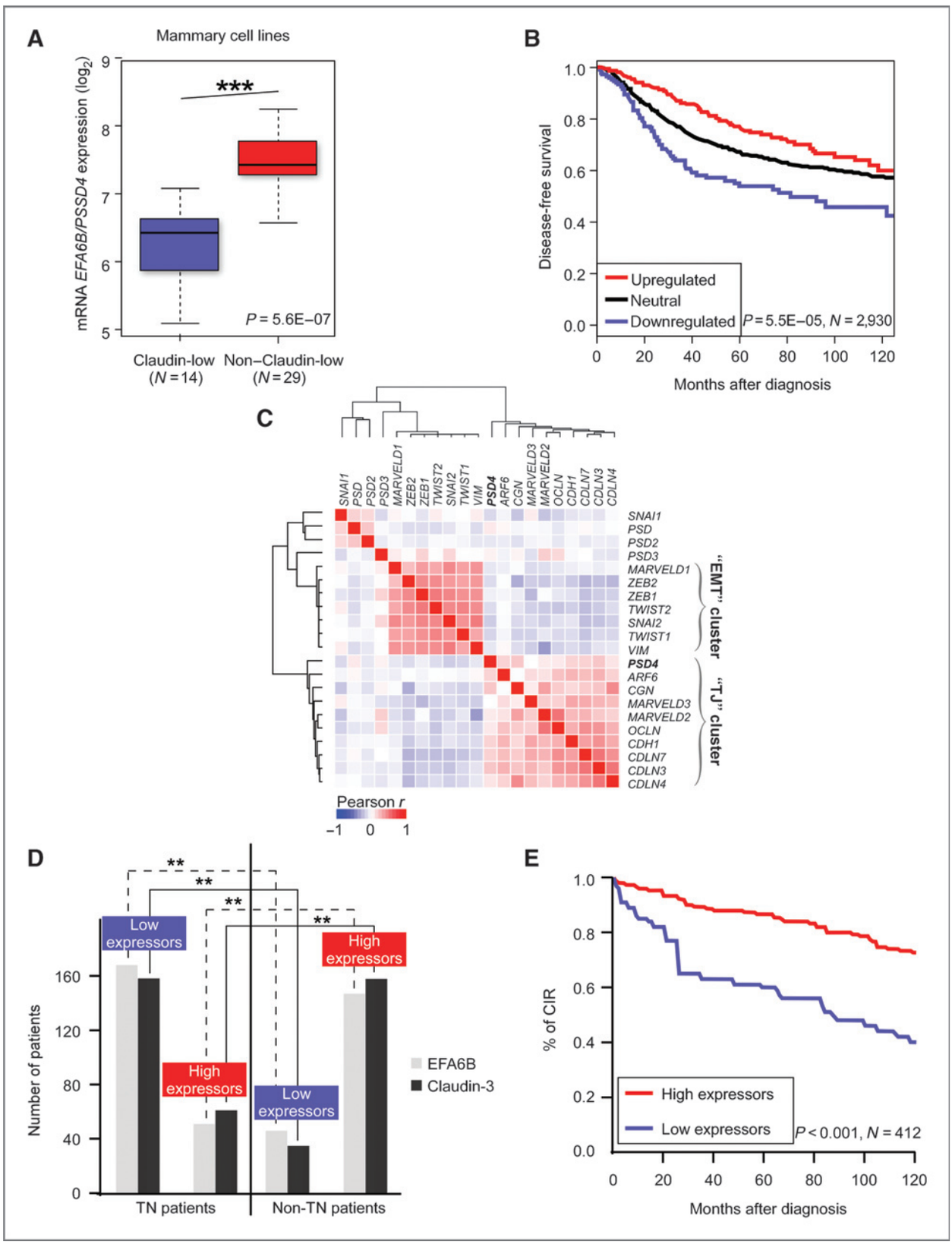

existed from downregulated to neutral to upregulated levels of *EFA6B*/*PSD4* (Table 1).

In agreement with the survival data, we found that tumors with *EFA6B*/*PSD4* downregulation were more frequently classified "high risk" of relapse by two major prognostic gene expression signatures, the Amsterdam 70-gene signature and the Oncotype Recurrence Score. Here too, a continuum was present between the three groups defined by *EFA6B*/*PSD4* expression (downregulation, neutral, and upregulation) and the above gene signatures (Table 1).

We next analyzed correlations between expression levels of *EFA6B*/*PSD4* and those of 20 genes involved in tight junction or EMT. As shown by the correlation matrix (Fig. 6C), *EFA6B*/*PSD4* expression positively correlated with that of genes involved in tight junction, including claudin genes, and negatively correlated with that of genes involved in EMT. Of note, the three other *EFA6*/*PSD* genes did not correlate with the "tight junction" and "EMT" gene clusters. We also found correlations between *EFA6B*/*PSD4* expression and gene expression signatures related to epithelial and mesenchymal phenotypes (Table 1). Tumors with *EFA6B*/*PSD4* downregulation had a higher expression score of the Stroma signature, the Stromal differentiation score, and the EMT score than tumors without no deregulation or tumors with upregulation. They also showed a differentiation score closer to mammary stem cells than mature luminal cells. Together with the low expression of tight junction genes and high expression of EMT genes, these findings are consistent with an EMT phenotype in the *EFA6B*/*PSD4*–downregulated tumors.

EFA6B and claudin-3 immunostaining expression in breast cancer

To extend the transcriptome analyses, we carried out IHC studies on human mammary tumor samples and assessed the protein levels of EFA6B in relation to the subtype and prognosis. We analyzed a collection 412 human primary invasive breast adenocarcinoma spotted onto a TMA. The Cld-low subtype has only been defined by gene profiling; nevertheless, *claudin-3* appears to be one of the most significantly affected genes in this subset (2, 34), so we quantified the levels of claudin-3 protein by IHC as a marker for the Cld-low subtype. We found a positive correlation between the presence of a triple-negative IHC for ER, PR, and HER2 and low expression of both EFA6B and claudin-3 proteins in primary breast tumors (Fig. 6D). Moreover, in tumors with a low expression of EFA6B, a low claudin-3 expression was concomitantly noted (Fig. 6D). Finally, patients with low levels of EFA6B expression correlated significantly with a lower DFS expressed as the cumulative incidence of relapse (Fig. 6E). Together with our transcriptomic analyses, these data showed that EFA6B is lost in aggressive mammary tumors downregulated in tight junction.

Discussion

We have provided evidence that the tight junction regulator EFA6B acts as an antagonist to human breast cancer development. *In vitro*, we have identified two biologic processes regulated by EFA6B through which it might hamper or even revert breast cancer progression: EFA6B inhibits the TGFβ-induced EMT, and EFA6B increases the formation and fusion of VACs to promote epithelial apico-basal polarity of mammary acinis. *In vivo*, breast cancer analyses show that loss of expression of EFA6B is a marker of poor prognosis and associated with the TNBC and Cld-low subtypes.

On the basis of these results and previous observations from us and others, we propose that *PSD4*/*EFA6B* is a new potential tumor suppressor and that an early loss of expression of EFA6B contributes to the malignant progression of breast cancer and might participate in the orientation toward the TNBC and Cld-low subtypes. Three lines of evidence corroborate this model: (i) *in vitro* manipulation of EFA6B levels affects the tight junction, the apico-basal polarity, and the EMT status of various tumoral and nontumoral human mammary cell lines: all properties that are shown to correlate, *in vivo*, with tumor progression and found to be necessary for tumor cell migration and invasion (35–38); (ii) likewise, *in vivo*, the gradual loss of expression of EFA6B correlates with a progressive increase in the appearance of breast cancer tumors characterized by a downregulation of the tight junction along with the emergence of an EMT signature; (iii) finally, loss of expression of EFA6B (mRNA and protein) in human mammary tumors is correlated with the formation of tumors of the Cld-low subtype primarily defined by a loss of tight junction and an upregulation of the EMT signature.

To further substantiate the antitumoral role of EFA6B, we set out to decipher the molecular mechanism(s) by which it reverted the MCF7 cell aggregates into normal-like mammary acinis in 3D culture. Our results demonstrate that EFA6B regulates both the formation of VACs, and lumens. The EFA6–Arf6 complex is known to control cell surface transport, therefore it is possible that EFA6B overexpression stimulates the formation of endocytic vesicles from the basal surface of the plasma membrane to form VACs, onto which EFA6B is localized, and then helps their subsequent fusion at cell–cell contacts to generate the lumens. Because the newly formed lumens are delineated by tight junctions, EF6AB might also

Figure 6. *EFA6B*/*PSD4* mRNA and EFA6B protein expression in breast cancer. A, box plots of *EFA6B*/*PSD4* expression across 43 human mammary cell lines according to the Cld-low or non–Cld-low subtype. Differences in expression levels between the two subtypes were tested for significance using Student *t* test. For each box plot, median and ranges are indicated. B, Kaplan–Meier DFS curves in patients with breast cancer according to *EFA6B*/*PSD4* mRNA expression; blue, downregulation; black, no deregulation; red, upregulation. Respective 5-year DFS are 54%, 67%, and 76% (log-rank test). C, correlation matrix for mRNA expression levels of 21 genes in 5,252 breast cancer. Pearson coefficients are color-coded according to the scale shown below the matrix. Genes are ordered according to hierarchical clustering of pairwise correlations. The dendrogram above and beside the matrix shows the degree of correlations. Three gene clusters are evidenced: EMT, tight junction (TJ), and PSDs. D, EFA6B and claudin-3 expression in breast triple-negative ($n = 219$) and non–triple-negative ($n = 193$) status for ER/PR/HER2. E, Kaplan–Meier curves of the cumulative incidence of relapse (CIR) stratified according to the differential expression of EFA6B 412 patients with breast cancer.

Table 1. Correlations between *PSD4* mRNA expression and histoclinical features of breast cancer samples or gene expression signatures in breast cancer samples

		PSD4 mRNA expression			
Characteristics	***N***	**Down (*N* = 281)**	**Neutral (*N* = 4,471)**	**Up (*N* = 500)**	***P***
Age at diagnosis, y					2.15E−02
≤50	1,654	82 (43%)	1,446 (46%)	126 (39%)	
>50	2,003	110 (57%)	1,692 (54%)	201 (61%)	
Histologic type					0.38
Ductal	1,355	98 (88%)	1,110 (82%)	147 (86%)	
Lobular	80	2 (2%)	71 (5%)	7 (4%)	
Other	196	11 (10%)	168 (13%)	17 (10%)	
Genomic Grade Index (GGI)					7,53E−08
Low	1,680	66 (29%)	1,418 (43%)	196 (53%)	
High	2,243	161 (71%)	1,906 (57%)	176 (47%)	
ESR1 status (mRNA level)					4.54E−23
Negative	2,000	173 (62%)	1,703 (38%)	124 (25%)	
Positive	3,252	108 (38%)	2,768 (62%)	376 (75%)	
PGR status (mRNA level)					2.75E−11
Negative	2,862	200 (71%)	2,434 (54%)	228 (46%)	
Positive	2,390	81 (29%)	2,037 (46%)	272 (54%)	
ERBB2 status (mRNA level)					0.0865
Negative	4,499	253 (90%)	3,823 (86%)	423 (85%)	
Positive	753	28 (10%)	648 (14%)	77 (15%)	
TN status (mRNA level)					4.12E−23
$ERBB2^+$	753	28 (10%)	648 (14%)	77 (15%)	
$HR^+/ERBB2^-$	3,097	110 (39%)	2,641 (59%)	346 (69%)	
TN	1,402	143 (51%)	1,182 (26%)	77 (15%)	
Molecular subtype (PAM50)					<1.0E−08
Basal	1,351	148 (53%)	1,149 (26%)	54 (11%)	
ERBB2-enriched	738	39 (14%)	639 (14%)	60 (12%)	
Luminal A	1,513	39 (14%)	1,261 (28%)	213 (43%)	
Luminal B	1,066	31 (11%)	905 (20%)	130 (26%)	
Normal	584	24 (9%)	517 (12%)	43 (9%)	
Cld-low signature					8.02E−14
Non–Cld-low	4,565	207 (74%)	3,889 (87%)	469 (94%)	
Cld-low	687	74 (26%)	582 (13%)	31 (6%)	
5-year DFS	2,930	54% [0.46–0.63]	67% [0.65–0.69]	76% [0.71–0.82]	5.47E−05
70-gene GES					2.47E−13
High risk	1,217	24 (9%)	1,037 (23%)	156 (31%)	
Low risk	4,035	257 (91%)	3,434 (77%)	344 (69%)	
Recurrence score					3.78E−22
High risk	2,387	176 (63%)	2,065 (46%)	146 (29%)	
Intermediate risk	1,024	56 (20%)	858 (19%)	110 (22%)	
Low risk	1,841	49 (17%)	1,548 (35%)	244 (49%)	
Stroma signature	5,116	0.19	−0.03	−0.24	1.07E−10
Differentiation score					
Stroma score	5,252	−0.04	−0.09	−0.21	5.7E−10
Mammary stem cell (MaSC)	5,252	0.19	−0.05	−0.27	3.17E−64
Progenitor luminal (pL)	5,252	−0.08	−0.27	−0.44	3.13E−27
Mature luminal (mL)	5,252	−0.35	0.03	0.3	8.08E−69
EMT metagene	5,252	−0.12	−0.16	−0.24	4.65E−03

Abbreviation: GES, gene expression signature.

help form the lumen by strengthening its surrounding tight junction, which have independently been shown to promote lumen formation (39).

In addition, the levels of expression of EFA6B determined the epithelial–mesenchymal morphologic status of MCF7 cell aggregates, which indicated that EFA6B might control EMT.

This is of primary importance because EMT has been largely implicated in carcinogenesis. TGFβ is a potent EMT-inducer of human mammary cancer (21, 37, 40). One of the earliest consequences of TGFβ binding to its receptor is the dissolution of the tight junction (26). Interestingly, exogenous expression of EFA6B blocked the TGFβ-induced EMT in MCF7 and MDCK cells. Preliminary examination of the major downstream effectors of TGFβ implicated in tight junction remodeling did not allow us to identify the signaling pathway(s) inhibited by EFA6B. In the past, we have shown that EFA6B and Arf6 control the tight junction by regulating the apical ring of acto-myosin (4, 41). Thus, the complex EFA6B–Arf6 may act directly on the apical tight junction actin ring, possibly counteracting or bypassing the effects of RhoA or other actin regulators.

Collectively, our results indicate that downregulation of EFA6B may contribute to breast cancer malignant progression. We tested this hypothesis by analyzing the expression of EFA6B in human breast tumor samples. Not only did we observe a reduced expression of EFA6B in human breast cancer, but in agreement with our *in vitro* studies, it was correlated with a decrease in tight junction components. This was associated with an increase in the signatures for EMT and CSC, and a lower DFS. The transcriptomic analysis showed that tumors with low EFA6B expression were more frequently of the Cld-low subtype. This breast cancer subtype is also defined by transcriptomic signatures associated with EMT and CSC, and a poor prognosis. Thus, collectively our transcriptomic, IHC, and *in vitro* data support a model whereby the loss of EFA6B might participate in the initiation or maintenance of the tight junction–downregulated Cld-low subtype. In any case, independent of a possible role of EFA6B on the subtype orientation, it is striking that the same biologic changes associated with EFA6B downregulation in human breast cancer and the ones induced by a decrease in EFA6B levels in cell culture—namely loss of tight junction and apico-basal polarity, increased EMT, stromal and CSC signatures—are all found in breast cancer tumoral progression.

In summary, EFA6B appears as a potential tumor antagonist whose downregulation may trigger the progression toward the Cld-low subtype. Inhibition of the mechanisms that downregulate EFA6B levels may offer a much needed therapeutic option.

Disclosure of Potential Conflicts of Interest

No potential conflicts of interest were disclosed.

Authors' Contributions

Conception and design: F. Luton
Development of methodology: J. Zangari, F. Bertucci, O. Cabaud, M. Lopez, P. Hofman, F. Luton
Acquisition of data (provided animals, acquired and managed patients, provided facilities, etc.): J. Zangari, M. Partisani, F. Bertucci, C. Berruyer-Pouyet, P. Finetti, E. Long, O. Cabaud, D. Birnbaum, M. Lopez, P. Hofman
Analysis and interpretation of data (e.g., statistical analysis, biostatistics, computational analysis): J. Zangari, F. Bertucci, G. Bidaut, P. Finetti, F. Brau, B. Chetaille, D. Birnbaum, M. Lopez, P. Hofman, M. Franco, F. Luton
Writing, review, and/or revision of the manuscript: F. Bertucci, P. Finetti, F. Luton
Administrative, technical, or material support (i.e., reporting or organizing data, constructing databases): J. Zangari, J. Milanini, M. Franco
Study supervision: F. Luton

Acknowledgments

The authors thank Drs. E. Van Obberghen-Schilling and J. Mazella for the generous gift of various reagents.

Grant Support

This work was supported by the Centre National de la Rechereche de Scientifique (CNRS) and the National Research Agency through the "Investments for the Future" LABEX SIGNALIFE (ANR-11-LABX-0028-01).

The costs of publication of this article were defrayed in part by the payment of page charges. This article must therefore be hereby marked *advertisement* in accordance with 18 U.S.C. Section 1734 solely to indicate this fact.

Received January 31, 2014; revised July 25, 2014; accepted July 28, 2014; published OnlineFirst August 12, 2014.

References

1. Sorlie T, Perou CM, Tibshirani R, Aas T, Geisler S, Johnsen H, et al. Gene expression patterns of breast carcinomas distinguish tumor subclasses with clinical implications. Proc Natl Acad Sci U S A 2001;98:10869–74.
2. Prat A, Parker JS, Karginova O, Fan C, Livasy C, Herschkowitz JI, et al. Phenotypic and molecular characterization of the claudin-low intrinsic subtype of breast cancer. Breast Cancer Res 2010;12:R68.
3. Prat A, Perou CM. Deconstructing the molecular portraits of breast cancer. Mol Oncol 2011;5:5–23.
4. Luton F, Klein S, Chauvin JP, Le Bivic A, Bourgoin S, Franco M, et al. EFA6, exchange factor for ARF6, regulates the actin cytoskeleton and associated tight junction in response to E-cadherin engagement. Mol Biol Cell 2004;15:1134–45.
5. Theard D, Labarrade F, Partisani M, Milanini J, Sakagami H, Fon EA, et al. USP9x-mediated deubiquitination of EFA6 regulates *de novo* tight junction assembly. EMBO J 2010;29:1499–509.
6. Debnath J, Mills KR, Collins NL, Reginato MJ, Muthuswamy SK, Brugge JS. The role of apoptosis in creating and maintaining luminal space within normal and oncogene-expressing mammary acini. Cell 2002;111:29–40.
7. Derrien V, Couillault C, Franco M, Martineau S, Montcourrier P, Houlgatte R, et al. A conserved C-terminal domain of EFA6-family ARF6-guanine nucleotide exchange factors induces lengthening of microvilli-like membrane protrusions. J Cell Sci 2002;115(Pt 14): 2867–79.
8. Macia E, Partisani M, Paleotti O, Luton F, Franco M. Arf6 negatively controls the rapid recycling of the beta2 adrenergic receptor. J Cell Sci 2012;125(Pt 17):4026–35.
9. Onder TT, Gupta PB, Mani SA, Yang J, Lander ES, Weinberg RA. Loss of E-cadherin promotes metastasis via multiple downstream transcriptional pathways. Cancer Res 2008;68:3645–54.
10. Marshansky V, Bourgoin S, Londoño I, Bendayan M, Vinay P. Identification of ADP-ribosylation factor-6 in brush-border membrane and early endosomes of human kidney proximal tubules. Electrophoresis 1997;18:538–47.
11. Luton F. The role of EFA6, exchange factor for Arf6, for tight junction assembly, functions, and interaction with the actin cytoskeleton. Methods Enzymol 2005;404:332–45.
12. Schneider CA, Rasband WS, Eliceiri KW. NIH Image to ImageJ: 25 years of image analysis. Nat Methods 2012;9:671–5.
13. Charafe-Jauffret E, Ginestier C, Monville F, Finetti P, Adelaide J, Cervera N, et al. Gene expression profiling of breast cell lines identifies potential new basal markers. Oncogene 2006;25:2273–84.
14. Han J, Chang H, Giricz O, Lee GY, Baehner FL, Gray JW, et al. Molecular predictors of 3D morphogenesis by breast cancer cell lines in 3D culture. PLoS Comput Biol 2010;6:e1000684.

15. Kenny PA, Lee GY, Myers CA, Neve RM, Semeiks JR, Spellman PT, et al. The morphologies of breast cancer cell lines in three-dimensional assays correlate with their profiles of gene expression. Mol Oncol 2007;1:84–96.
16. Vega-Salas DE, Salas PJ, Rodriguez-Boulan E. Modulation of the expression of an apical plasma membrane protein of Madin–Darby canine kidney epithelial cells: cell–cell interactions control the appearance of a novel intracellular storage compartment. J Cell Biol 1987; 104:1249–59.
17. Vega-Salas DE, Salas PJ, Rodriguez-Boulan E. Exocytosis of vacuolar apical compartment (VAC): a cell–cell contact controlled mechanism for the establishment of the apical plasma membrane domain in epithelial cells. J Cell Biol 1988;107:1717–28.
18. Vega-Salas DE, San Martino JA, Salas PJ, Baldi A. Vacuolar apical compartment (VAC) in breast carcinoma cell lines (MCF-7 and T47D): failure of the cell–cell regulated exocytosis mechanism of apical membrane. Differentiation 1993;54:131–41.
19. Debnath J, Brugge JS. Modelling glandular epithelial cancers in three-dimensional cultures. Nat Rev Cancer 2005;5:675–88.
20. Manuel Iglesias J, Beloqui I, Garcia-Garcia F, Leis O, Vazquez-Martin A, Eguiara A, et al. Mammosphere formation in breast carcinoma cell lines depends upon expression of E-cadherin. PLoS ONE 2013;8: e77281.
21. Barcellos-Hoff MH, Akhurst RJ. Transforming growth factor-beta in breast cancer: too much, too late. Breast Cancer Res 2009;11:202.
22. Padua D, Massague J. Roles of TGFbeta in metastasis. Cell Res 2009;19:89–102.
23. Parvani JG, Taylor MA, Schiemann WP. Noncanonical TGF-beta signaling during mammary tumorigenesis. J Mammary Gland Biol Neoplasia 2011;16:127–46.
24. Ikenouchi J, Matsuda M, Furuse M, Tsukita S. Regulation of tight junctions during the epithelium-mesenchyme transition: direct repression of the gene expression of claudins/occludin by Snail. J Cell Sci 2003;116(Pt 10):1959–67.
25. Medici D, Hay ED, Goodenough DA. Cooperation between snail and LEF-1 transcription factors is essential for TGF-beta1–induced epithelial–mesenchymal transition. Mol Biol Cell 2006;17:1871–9.
26. Viloria-Petit AM, Wrana JL. The TGFbeta-Par6 polarity pathway: linking the Par complex to EMT and breast cancer progression. Cell Cycle 2010;9:623–4.
27. Vincent T, Neve EP, Johnson JR, Kukalev A, Rojo F, Albanell J, et al. A SNAIL1-SMAD3/4 transcriptional repressor complex promotes TGF-beta mediated epithelial–mesenchymal transition. Nat Cell Biol 2009; 11:943–50.
28. Xu J, Lamouille S, Derynck R. TGF-beta–induced epithelial to mesenchymal transition. Cell Res 2009;19:156–72.
29. Kong W, Yang H, He L, Zhao JJ, Coppola D, Dalton WS, et al. MicroRNA-155 is regulated by the transforming growth factor beta/Smad pathway and contributes to epithelial cell plasticity by targeting RhoA. Mol Cell Biol 2008;28:6773–84.
30. Ozdamar B, Bose R, Barrios-Rodiles M, Wang HR, Zhang Y, Wrana JL. Regulation of the polarity protein Par6 by TGFbeta receptors controls epithelial cell plasticity. Science 2005;307:1603–9.
31. Wu G, Xing M, Mambo E, Huang X, Liu J, Guo Z, et al. Somatic mutation and gain of copy number of PIK3CA in human breast cancer. Breast Cancer Res 2005;7:R609–16.
32. Yuan TL, Cantley LC. PI3K pathway alterations in cancer: variations on a theme. Oncogene 2008;27:5497–510.
33. Cerami E, Gao J, Dogrusoz U, Gross BE, Sumer SO, Aksoy BA, et al. The cBio cancer genomics portal: an open platform for exploring multidimensional cancer genomics data. Cancer Discov 2012;2: 401–4.
34. Herschkowitz JI, Simin K, Weigman VJ, Mikaelian I, Usary J, Hu Z, et al. Identification of conserved gene expression features between murine mammary carcinoma models and human breast tumors. Genome Biol 2007;8:R76.
35. Brennan K, Offiah G, McSherry EA, Hopkins AM. Tight junctions: a barrier to the initiation and progression of breast cancer? J Biomed Biotechnol 2010;2010:460607.
36. Tanos B, Rodriguez-Boulan E. The epithelial polarity program: machineries involved and their hijacking by cancer. Oncogene 2008;27: 6939–57.
37. Taylor MA, Parvani JG, Schiemann WP. The pathophysiology of epithelial–mesenchymal transition induced by transforming growth factor-beta in normal and malignant mammary epithelial cells. J Mammary Gland Biol Neoplasia 2010;15:169–90.
38. Thiery JP, Sleeman JP. Complex networks orchestrate epithelial–mesenchymal transitions. Nat Rev Mol Cell Biol 2006;7:131–42.
39. Ferrari A, Veligodskiy A, Berge U, Lucas MS, Kroschewski R. ROCK-mediated contractility, tight junctions and channels contribute to the conversion of a preapical patch into apical surface during isochoric lumen initiation. J Cell Sci 2008;121(Pt 21):3649–63.
40. Yu M, Bardia A, Wittner BS, Stott SL, Smas ME, Ting DT, et al. Circulating breast tumor cells exhibit dynamic changes in epithelial and mesenchymal composition. Science 2013;339:580–4.
41. Klein S, Partisani M, Franco M, Luton F. EFA6 facilitates the assembly of the tight junction by coordinating an Arf6-dependent and -independent pathway. J Biol Chem 2008;283:30129–38.